ARCHIVES OF ELECTRICAL ENGINEERING VOL. 71(2), pp. 343–362 (2022)

DOI 10.24425/aee.2022.140715

Predictive current control for permanent magnet synchronous motor based on internal model control observer

MIN'AN TANG, CHENYU WANG, YINHANG LUO ✉

School of Automation and Electrical Engineering, Lanzhou Jiaotong University
China No. 88, Anning West Road, Anning District, Lanzhou City, Gansu Province, China
e-mails: {lzjtdx508/18205180633/✉wcy794730778}@163.com

(Received: 13.07.2021, revised: 15.11.2021)

Abstract: The model predictive current control (MPCC) of the permanent magnet synchronous motor (PMSM) is highly dependent on motor parameters, and a parameter mismatch will cause the system performance degradation. Therefore, a strategy based on an internal model control (IMC) observer is proposed to correct the mismatch parameters. Firstly, based on the MPCC strategy of the PMSM, according to the dynamic model of the PMSM in a rotating orthogonal coordinate system, d-axis and q-axis current IMC observers are designed, and the stability derivation is carried out. It is proved that the observer can estimate d-axis and q-axis disturbance components caused by a parameter mismatch without static error. Then, the estimated disturbance component is compensated for by the reference voltage prediction expression. Finally, the effectiveness of the proposed strategy is verified in two different conditions. The experimental results show that the proposed control strategy can effectively compensate for the parameter mismatch disturbance in MPCC for PMSM, improve the dynamic and static performance of the system, and improve the robustness of the system.

Key words: internal model control observer, MPC, PMSM, predictive current control

1. Introduction

Permanent magnet synchronous motors (PMSMs) are highly efficient, energy-saving, structurally diverse, and high in starting torque, which explains their extensive applications in various industries and fields, such as petroleum, rail transit, and household appliances [1–3]. Currently, model predictive control (MPC) is a research focus in motor control due to its flexible principle of

© 2022. The Author(s). This is an open-access article distributed under the terms of the Creative Commons Attribution-NonCommercial-NoDerivatives License (CC BY-NC-ND 4.0, https://creativecommons.org/licenses/by-nc-nd/4.0/), which permits use, distribution, and reproduction in any medium, provided that the Article is properly cited, the use is non-commercial, and no modifications or adaptations are made.

www.czasopisma.pan.pl PAN POLSKA AKADEMIA NAUK www.journals.pan.pl

optimality, good robustness, and efficiency when it comes to solving nonlinear and multivariable problems [4–6].

MPC for the PMSM is a control algorithm that is significantly dependent on parameters. A model mismatch will affect the precision and accuracy of motor control, causing calculation errors in the time of vector effects, among many others [7–9]. At present, to address the problem of degraded MPC strategic performance arising from a model mismatch, many scholars have proposed a number of countermeasures. In [10], authors used identified motor parameters to correct parameters of the predictive model in real time. This measure introduces ordinary least squares (OLS) to identify the motor parameters, but OLS computation is very time consuming, which makes it unsuitable for real-time identification [11, 12]. In [13], authors converted OLS into a recursive algorithm allowing it to store only a part of the data for identification, thus making real-time identification achievable. Yet, the recursive least squares (RLS) algorithm is poor in tracking the time-varying environment, not to mention that it is vulnerable to noise, which may lead to a larger error in model parameter estimation. Another alternative is to combine predictive control with intelligent control. Predictive control based on neural network error correction can better inhibit a model mismatch but tends to suffer from the slow convergence rates of neural networks, preventing them from quick adaptation to environments with variable operating conditions [14, 15]. The feedback compensation for error from a model mismatch by fuzzy inference also offers a viable path [16, 17] but tends to be disadvantaged by a less systematic fuzzy control design. The last countermeasure would be to perform an early estimation of predictive error caused by a model mismatch, before including the corresponding error compensation in the MPC strategy [18, 19]. By building the error model of each step and the transitive relationship of errors, independent error compensation schemes for each step can be developed. However, the estimation of predictive error increases the system's computation burden and reduces system efficiency.

To solve the problem of degraded predictive control performance caused by a motor model mismatch, on top of the three-vector model predictive current control (MPCC) for the PMSM, this paper proposes a model parametric mismatch countermeasure based on an internal model control (IMC) observer [20]. To begin with, the IMC observer was designed according to the dynamic model of the PMSM in a rotating orthogonal coordinate system. The stabilities of the designed IMC observer on d-axis and q-axis currents were then derived and verified, proving the effectiveness of the observer in estimating the component of parametric-mismatch-caused disturbance along the d and q axes. After that, the estimated disturbance component is compensated for by the reference voltage prediction expression. In the end, the strategy is applied in the PMSM three-vector MPCC. According to the experiment, the strategy herein can compensate for the disturbance of a parametric mismatch in real time, thus improving the system robustness.

2. Three-vector MPCC of PMSM

2.1. Mathematical model of the PMSM

The model for the surface-mounted PMSM in the rotating orthogonal coordinate system (d-q) can be expressed as:

$$\begin{cases} \dfrac{\mathrm{d}i_d}{\mathrm{d}t} = \dfrac{1}{L_d}\left(u_d - Ri_d + \omega_e L_q i_q\right) \\ \dfrac{\mathrm{d}i_q}{\mathrm{d}t} = \dfrac{1}{L_q}\left(u_q - Ri_q - \omega_e L_d i_d - \omega_e \psi_f\right) \end{cases}, \tag{1}$$

where: L_d and L_q are the direct-axis and quadrature-axis components of stator inductance, respectively, $L_d = L_q = L$; i_d, i_q, u_d and u_q are the direct-axis and quadrature-axis components of the stator current and voltage, respectively; R is the stator resistance; ω_e is the rotor electrical angular speed, and ψ_f is the rotor permanent magnet flux linkage.

According to Expression (1), taking stator current as a variable of state, the state-space model can be re-expressed as:

$$\frac{\mathrm{d}\boldsymbol{i}}{\mathrm{d}t} = \boldsymbol{A}\,\boldsymbol{i} + \boldsymbol{B}\,\boldsymbol{u} + \boldsymbol{C}, \tag{2}$$

where:

$$\boldsymbol{A} = \begin{bmatrix} -R/L & \omega_e \\ -\omega_e & -R/L \end{bmatrix}, \qquad \boldsymbol{B} = \begin{bmatrix} 1/L & 0 \\ 0 & 1/L \end{bmatrix}, \qquad \boldsymbol{C} = \begin{bmatrix} 0 \\ -\psi_f\,\omega_e/L \end{bmatrix},$$

$$\boldsymbol{i} = \left[i_d,\ i_q\right]^T, \qquad \boldsymbol{u} = \left[u_d,\ u_q\right]^T.$$

2.2. The principle of three-vector MPCC

The so-called "three vectors" refer to the three basic space voltage vectors, which include two effective voltage vectors and one zero-vector. The effective voltage vectors are (100), (110), (010), (011), (001) and (101), while the zero-vectors are (000) and (111).

Figure 1 is the structure diagram of the three-vector MPCC of the PMSM, showing mainly the predictive current, calculation of time of vector effect, value function optimization and other modules. The given current in the system is $i_d^* = 0$; the given current i_q^* is the output of a velocity loop PI controller. Among others, u_i and u_j are two effective voltage vectors, which, together with the zero-vector, form the resultant voltage vector u_{dq}-control variable of the PMSM.

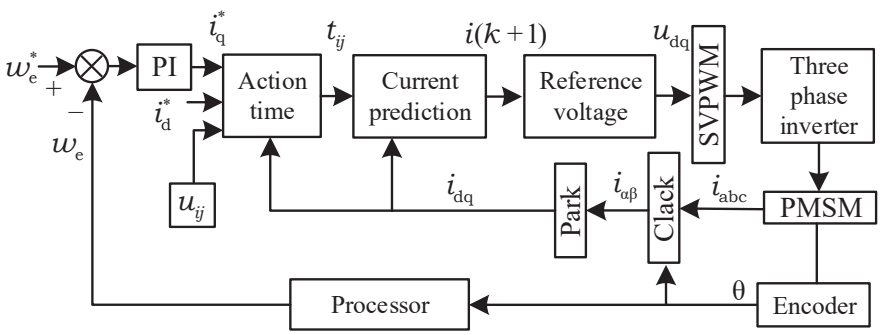

Fig. 1. Block diagram of the three-vector-based model predictive current control system

2.3. Predictive current

By discretizing the equation of state (2) with the Euler method, the expression of delay compensation of d-axis and q-axis currents can be expressed as:

$$\boldsymbol{i}^p(k+1) = \boldsymbol{A}(k)\boldsymbol{i}(k) + \boldsymbol{B}(k)\boldsymbol{u}(k) + \boldsymbol{C}(k), \tag{3}$$

www.czasopisma.pan.pl PAN POLSKA AKADEMIA NAUK www.journals.pan.pl

where:

$$\boldsymbol{i}^p(k+1) = \left[i_d^p(k+1), i_q^p(k+1)\right]^T, \quad \boldsymbol{i}(k) = \left[i_d(k),\ i_q(k)\right]^T, \quad \boldsymbol{u}(k) = \left[u_d(k),\ u_q(k)\right]^T,$$

$$\boldsymbol{A}(k) = \begin{bmatrix} 1 - T_s R/L & T_s\omega_e(k) \\ -T_s\omega_e(k) & 1 - T_s R/L \end{bmatrix}, \quad \boldsymbol{B}(k) = \begin{bmatrix} T_s/L & 0 \\ 0 & T_s/L \end{bmatrix}, \quad \boldsymbol{C}(k) = \begin{bmatrix} 0 \\ -T_s\psi_f\,\omega_e(k)/L \end{bmatrix}.$$

In Formula (3), $\boldsymbol{i}(k)$ is the sampled value of current in the kth period; $\boldsymbol{i}^p(k+1)$ is the predicted value of current of the $(k+1)^{\text{th}}$ period; T_s is the sampling period; $\boldsymbol{u}(k)$ is the sampled value of voltage in the kth period, which is worked out in the $(k-1)^{\text{th}}$ period; $\omega_e(k)$ is the sampled value of rotor electrical angular speed in the kth period.

The following is the computation formula for stator voltage applied onto surface-mounted PMSMs at $t(k+1)$ in the $d-q$ rotating coordinate system using the deadbeat current control:

$$\begin{cases} u_d^*(k+1) = Ri_d^p(k+1) + L\dfrac{i_d^* - i_d^p(k+1)}{T_s} - \omega_e(k)Li_q^p(k+1) \\ u_q^*(k+1) = Ri_q^p(k+1) + L\dfrac{i_q^* - i_q^p(k+1)}{T_s} + \omega_e(k)Li_d^p(k+1) + \omega_e(k)\psi_f \end{cases}. \tag{4}$$

In two-phase stationary coordinate system, determine the sector n where the complex vector is located, and calculate the position angle θ_p of the complex vector in the sector. The relationship expression between n and θ_p is

$$\theta_p = \arcsin\left(\frac{u_\beta}{u_\alpha}\right) - \frac{(n-1)\pi}{3}. \tag{5}$$

The position angle of the reference voltage vector is shown in Fig. 2.

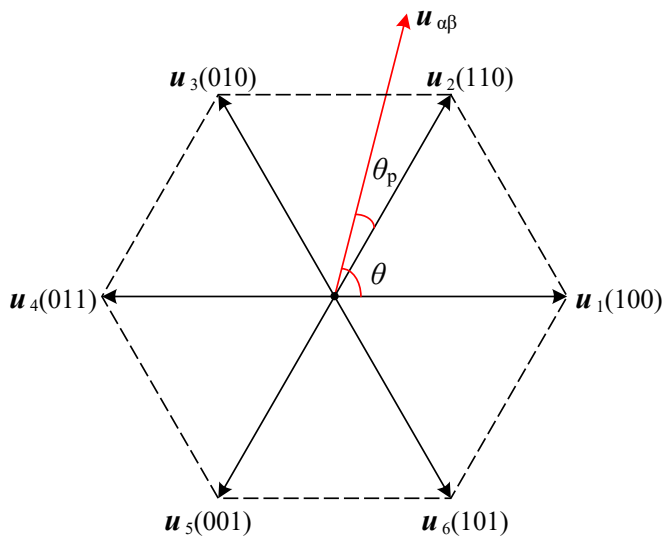

Fig. 2. Schematic diagram of reference voltage vector position angle

For convenience, note

$$|u^*| = \sqrt{u_d^{*2} + u_q^{*2}},$$

and the expression of reference voltage vector amplitude correction u_{dq}^* is

$$\begin{cases} u_d^{\text{opt}} = \begin{cases} \dfrac{V_{\text{dc}} u_d^*}{\sqrt{3}\sin\left(\dfrac{\pi}{3} + \theta_p\right)|u^*|}, & |u^*| > \dfrac{V_{\text{dc}}}{\sqrt{3}\sin\left(\dfrac{\pi}{3} + \theta_p\right)} \\ u_d^*, & 0 < |u^*| \le \dfrac{V_{\text{dc}}}{\sqrt{3}\sin\left(\dfrac{\pi}{3} + \theta_p\right)} \end{cases} \\ u_q^{\text{opt}} = \begin{cases} \dfrac{V_{\text{dc}} u_q^*}{\sqrt{3}\sin\left(\dfrac{\pi}{3} + \theta_p\right)|u^*|}, & |u^*| > \dfrac{V_{\text{dc}}}{\sqrt{3}\sin\left(\dfrac{\pi}{3} + \theta_p\right)} \\ u_q^*, & 0 < |u^*| \le \dfrac{V_{\text{dc}}}{\sqrt{3}\sin\left(\dfrac{\pi}{3} + \theta_p\right)} \end{cases} \end{cases}. \tag{6}$$

u_d^{opt} and u_q^{opt} are the voltage vectors after amplitude correction. If they are taken as the given voltage of the inverter, the actual voltage of the inverter is u_d^{opt} and u_q^{opt}. The two basic voltage vectors and zero vectors adjacent to the sector n, where the reference voltage complex vector is located are the three vectors required for control. Note

$$|u| = \sqrt{\left(u_d^{\text{opt}}\right)^2 + \left(u_q^{\text{opt}}\right)^2},$$

then the action time expression of the three vectors is

$$\begin{cases} t_i^{\text{opt}} = \dfrac{\sqrt{3} T_s |u| \sin\left(\dfrac{\pi}{3} - \theta_p\right)}{V_{\text{dc}}} \\ t_j^{\text{opt}} = \dfrac{\sqrt{3} T_s |u| \sin\left(\theta_p\right)}{V_{\text{dc}}} \\ t_j^{\text{opt}} = T_s - t_i^{\text{opt}} - t_j^{\text{opt}} \end{cases}. \tag{7}$$

3. The three-vector MPCC with online model parameter correction

3.1. Design of IMC observer

Under actual working conditions, control systems face inevitable parameter disturbance, such as model mismatch between the model of the control system and the actual system. Therefore, the algorithm-based predictive trajectory may deviate from the actual trajectory of system operation, potentially causing system performance degradation or even system instability. The following part introduces an IMC-based observer to address the model parametric mismatch. Subject to changes in actual motor parameters, the mathematical model of a surface-mounted PMSM can

www.czasopisma.pan.pl PAN POLSKA AKADEMIA NAUK www.journals.pan.pl

be re-expressed as:

$$\begin{cases} \dfrac{\mathrm{d}i_d}{\mathrm{d}t} = \dfrac{1}{(L+\Delta L)}\left(u_d - (R+\Delta R)i_d + \omega_e(L+\Delta L)i_q\right) \\ \dfrac{\mathrm{d}i_q}{\mathrm{d}t} = \dfrac{1}{(L+\Delta L)}\left(u_q - (R+\Delta R)i_q - \omega_e(L+\Delta L)i_d - \omega_e(\psi_f + \Delta\psi_f)\right) \end{cases}, \tag{8}$$

where: L, R and ψ_f stand for the model parameter of stator inductance, stator resistance and permanent magnet flux linkage, respectively; ΔL, ΔR and $\Delta\psi_f$ are the corresponding deviation.

f_d and f_q are defined to be the deviation of the rate of current change along the d-axis and q-axis, respectively, in the model mismatch system.

$$\begin{cases} f_d = \Delta L\dfrac{\mathrm{d}i_d}{\mathrm{d}t} + \Delta R i_d - \omega_e \Delta L i_q \\ f_q = \Delta L\dfrac{\mathrm{d}i_q}{\mathrm{d}t} + \Delta R i_q + \omega_e \Delta L i_d + \omega_e \Delta\psi_f \end{cases}. \tag{9}$$

As such, Formula (8) can be simplified to:

$$\frac{\mathrm{d}i_d}{\mathrm{d}t} = \frac{1}{L}\left(u_d - Ri_d + \omega_e L i_q - f_d\right), \tag{10}$$

$$\frac{\mathrm{d}i_q}{\mathrm{d}t} = \frac{1}{L}\left(u_q - Ri_q - \omega_e L i_d - \omega_e\psi_f - f_q\right). \tag{11}$$

In Formula (10), taking i_d as the variable of state, the equation of state becomes:

$$\begin{cases} \dot{x} = ax + b(u-d) \\ y = x \end{cases}, \tag{12}$$

where: $x = i_d$, $a = -\dfrac{R}{L}$, $b = \dfrac{1}{L}$, $u = u_d + \omega_e L i_q$, $d = f_d$.

In Formula (12), factors a and b can be readily obtainable. The state estimation system of the original system was then constructed to facilitate the acquisition of the original system's coefficient from the coefficient of state estimation. The state estimation equation is:

$$\begin{cases} \dot{\hat{x}} = a\hat{x} + b(u-\hat{d}) \\ \hat{y} = \hat{x} \end{cases}, \tag{13}$$

where $\hat{x}$ and $\hat{d}$ are the estimations of the variable of state x and the estimation of the deviation d. Assuming the error of the state variable $\widetilde{x} = x - \hat{x}$, then the error of deviation would be $\widetilde{d} = \hat{d} - d$.

By subtracting (12) from (13), the state equation with the error $\widetilde{x}$ as the variable of state can be expressed as:

$$\begin{cases} \dot{\widetilde{x}} = a\widetilde{x} + b\widetilde{d} \\ y - \hat{y} = \widetilde{x} \end{cases}. \tag{14}$$

The error $\widetilde{d}$ is taken as a system input or control variable. Theoretically, when the initial value of the original system is the same as that of the reconstructed system, $x = \hat{x}$ and $d = \hat{d}$. But in

fact, it's very hard to make sure their initial values are identical, i.e., $x \neq \hat{x}$. When $x \neq \hat{x}$, $y \neq \hat{y}$. Therefore, the feedback signal $\widetilde{y} = y - \hat{y}$ is introduced to form a closed-loop system. According to the design principle of IMC, a system whose reference input is equal to 0 can be designed, with the following error e of Formula (14) being:

$$\begin{cases} e = 0 - \widetilde{y} \\ \dot{e} = -\dot{\widetilde{y}} = -\dot{\widetilde{x}} \end{cases}. \tag{15}$$

Introducing a new variable of state $z = \dot{\widetilde{x}}$ to Formula (14), we have:

$$\dot{z} = \ddot{\widetilde{x}} = az + b\dot{\widetilde{d}}. \tag{16}$$

(15) and (16) constitute the state space equation group:

$$\begin{bmatrix} \dot{e} \\ \dot{z} \end{bmatrix} = \begin{bmatrix} 0 & -1 \\ 0 & a \end{bmatrix} \begin{bmatrix} e \\ z \end{bmatrix} + \begin{bmatrix} 0 \\ b \end{bmatrix} \dot{\widetilde{d}} \quad \rightarrow \quad \dot{Z} = \boldsymbol{A}\,\boldsymbol{Z} + \boldsymbol{B}\dot{\widetilde{d}}, \tag{17}$$

where: $\boldsymbol{A} = [0, -1;\ 0, a]$, $\boldsymbol{B} = [0, b]^T$. In (14), $\text{rank}[\boldsymbol{B}\ \boldsymbol{AB}] = 2$, the rank of the matrix is apparently equal to the number of rows, i.e., the system represented by (17) is fully controllable. Feedback $\dot{\widetilde{d}} = -\boldsymbol{KZ}$ was then introduced to the randomly set eigenvalue of the system. In $\dot{\widetilde{d}} = -\boldsymbol{KZ}$, $\boldsymbol{K} = [k_1,\ k_2]$, so that controlled Formula (17) may achieve asymptotical stability. According to (15) and (16), the control variable $\dot{\widetilde{d}}$:

$$\dot{\widetilde{d}} = -k_1 e - k_2 z = k_1\widetilde{x} - k_2\dot{\widetilde{x}}, \tag{18}$$

where k_1 and k_2 are the parameters to be designed. The system properties can be modified by the reasonable design of the values k_1 and k_2. When the sampling period T_s of the control system is negligible, assuming that the value of the parameter d is constant, $\dot{d} = 0$, and Formula (18) can be further expressed as:

$$\dot{\hat{d}} = k_1\widetilde{x} - k_2\dot{\widetilde{x}}. \tag{19}$$

The eigenvalue of the state feedback system can be obtained from the eigenfunction

$$\det\left[s\boldsymbol{I} - (\boldsymbol{A} - \boldsymbol{BK})\right] = 0.$$

Let the system eigenvalue be the eigenvalue of a typical second-order system

$$-\xi\omega_n \pm \mathrm{j}\omega_n\sqrt{1-\xi^2}\,,$$

where: ζ is the damping ratio; ω_n is the undamped oscillating frequency. System performance can be improved by selecting the appropriate ζ and ω_n values. The eigenvalue can be further determined to obtain the observer parameters k_1 and k_2:

$$\begin{cases} k_1 = -\dfrac{\omega_n^2}{b} \\ k_2 = \dfrac{a + 2\zeta\omega_n}{b} \end{cases}. \tag{20}$$

Stability analysis

According to the principle of state feedback, Formula (17) is under the constraint of feedback parametric Expression (19) [21]; when the system operation time $t \to \infty$, i.e., the system is at a steady state, the stability value of the state vector Z in (17): $Z_s \to$, therefore, the stability values of the corresponding variables e and z: $e_s \to$, $z_s \to$. According to (14)–(16), at a steady state, the error of the state variable $\widetilde{x}_s \to$, $\dot{\widetilde{x}}_s \to$. Substituting $\widetilde{x}_s$ and $\dot{\widetilde{x}}_s \to$ into (14), it can be learned that at a steady state, the deviation error $\widetilde{d}_s \to$, therefore, $\hat{d}_s = d_s = \hat{f}_d$, i.e.,

$$\dot{\hat{f}}_d = \dot{\hat{d}} = k_1\widetilde{x} - k_2\dot{\widetilde{x}}. \tag{21}$$

3.2. Estimation of system parameters

Formulas (13) and (21) constitute the equation set of the d-axis current of the IMC observer, i.e.,

$$\begin{cases} \hat{i}_d = \displaystyle\int_0^T -\frac{R}{L}\hat{i}_d + \frac{1}{L}\left(u_d + \omega_e L i_q - \hat{f}_d\right) \mathrm{d}t \\ \dot{\hat{f}}_d = k_1\left(i_d - \hat{i}_d\right) - k_2\left(\dot{i}_d - \dot{\hat{i}}_d\right) \end{cases}. \tag{22}$$

From $\dot{d} = 0$, we have $\dot{\hat{d}}_s = \dot{f}_d = 0$, $k_1 \neq 0$ and $k_2 \neq 0$ in (22). Therefore, $i_d = \hat{i}_d$, $\dot{i}_d = \dot{\hat{i}}_d$.

Obviously, the IMC observer can be used to estimate the state variable of the original system without the presence of static error.

Likewise, the q-axis current equation set of the IMC observer is similar to its d-axis counterpart, specifically as follows:

$$\begin{cases} \hat{i}_q = \displaystyle\int_0^T -\frac{R}{L}\hat{i}_q + \frac{1}{L}\left(u_q - \omega_e L i_d - \omega_e \psi_f - \hat{f}_q\right) \mathrm{d}t \\ \dot{\hat{f}}_q = k_1\left(i_q - \hat{i}_q\right) - k_2\left(\dot{i}_q - \dot{\hat{i}}_q\right) \end{cases}. \tag{23}$$

Similarly, $\dot{\hat{d}}_s = \dot{f}_q = 0$, $k_1 \neq 0$ and $k_2 \neq 0$, therefore, $i_q = \hat{i}_q$, $\dot{i}_q = \dot{\hat{i}}_q$. According to the above analysis, the IMC observer can be used to estimate d-axis and q-axis stator currents of the motor and its rate of change under zero steady-state error. Figure 3 shows the structural diagram of d-axis and q-axis stator currents of the motor, as estimated by the IMC observer.

Then, the expression of the disturbance component from the mismatch parameter should be:

$$\begin{cases} \hat{f}_d = \displaystyle\int k_1\left(i_d - \hat{i}_d\right) - k_2\left(\dot{i}_d - \dot{\hat{i}}_d\right) \mathrm{d}t \\ \hat{f}_q = \displaystyle\int k_1\left(i_q - \hat{i}_q\right) - k_2\left(\dot{i}_q - \dot{\hat{i}}_q\right) \mathrm{d}t \end{cases}. \tag{24}$$

By compensating the disturbance component to the reference voltage Expression (4), the revised computation formula for stator voltage at $t+1$ can be expressed as follows:

$$\begin{cases} u_d^*(k+1) = R i_d^p(k+1) + L\dfrac{i_d^* - i_d^p(k+1)}{T_s} - \omega_e(k) L i_q^p(k+1) + f_d \\ u_q^*(k+1) = R i_q^p(k+1) + L\dfrac{i_q^* - i_q^p(k+1)}{T_s} + \omega_e(k) L i_d^p(k+1) + \omega_e(k)\psi_f + f_q \end{cases}. \tag{25}$$

www.czasopisma.pan.pl PAN POLSKA AKADEMIA NAUK www.journals.pan.pl

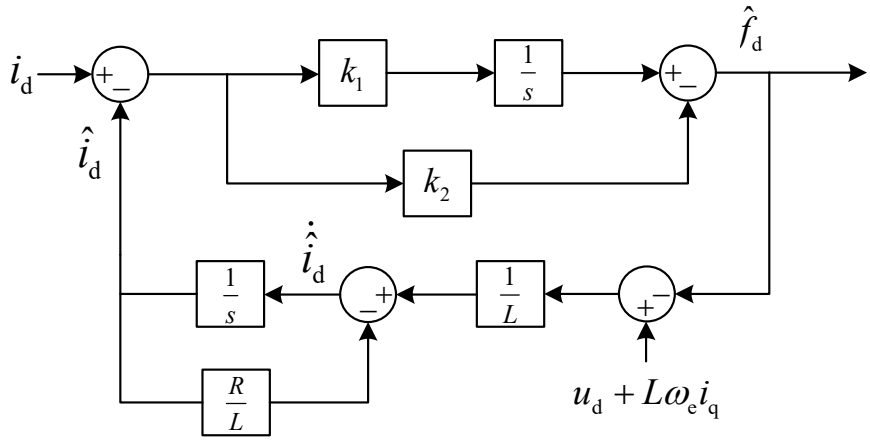

(a) IMC observer of d-axis current

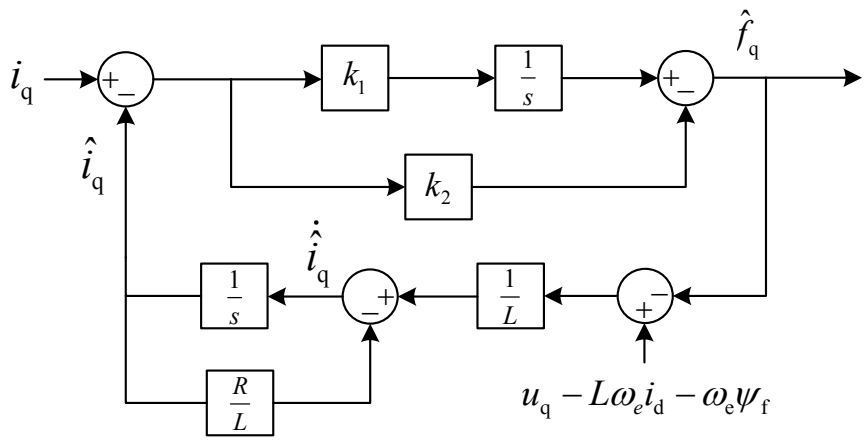

(b) IMC observer of q-axis current

Fig. 3. Structure diagram of d-axis and q-axis IMC observer

3.3. IMC observer-based countermeasure against model mismatch

Figure 4 shows the diagram of the IMC-observer-based countermeasure against the model mismatch. Based on the sampled stator current, d-axis and q-axis currents can be obtained, while the estimation disturbance caused by mismatched parameters can be acquired from the IMC observer. The estimated disturbance could then be fed back to the MPC module to attain the optimal switching tube state within a sampling period. In this way, the output current could be pushed as close to the given current as possible.

Figure 5 shows the diagram of IMC-observer-based PMSM three-vector MPCC. Unlike traditional PMSM three-vector MPCC systems, an online estimation disturbance was introduced before computing the module at the time of effect, using the said estimation disturbance to correct the model.

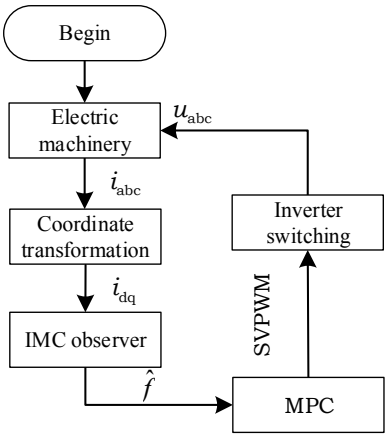

Fig. 4. Block diagram of model mismatch strategy based on internal model control observer

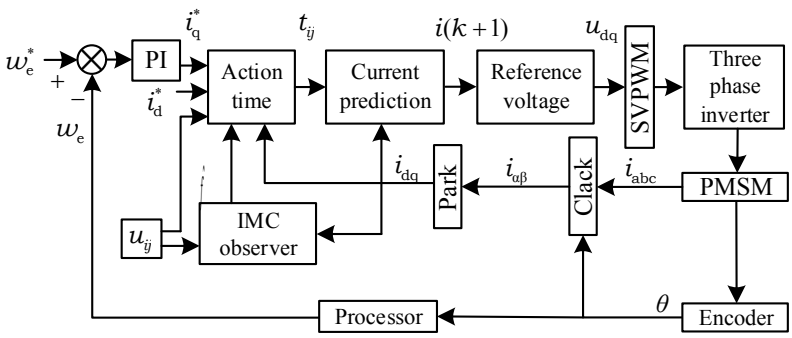

Fig. 5. Block diagram of model predictive current control based on internal model control observer

3.4. Kalman filter system

In practical application, the estimation of motor stator current is often disturbed by the internal and external boundaries, which cause the interference signal to be superimposed on the useful signal, so it is necessary to eliminate or weaken the interference noise from the parameter estimation data and extract the optimal parameter estimation. Therefore, the current estimation in Formula (24) is obtained from the real-time observation data of the IMC observer and processed by the Kalman filter.

Considering that the filter system has no control quantity, the discrete Kalman filter system equation can be simplified to

$$x_{k+1} = \boldsymbol{A}x_k + w_k\,, \tag{26}$$

$$z_k = \boldsymbol{H}x_k + v_k\,, \tag{27}$$

where: x_k is the parameter estimation vector of the discrete time series k; z_k is the observation vector of the discrete time series k; both matrix A and matrix H are the known square matrices; vector w_k and vector v_k represent process noise and observation noise, respectively.

www.czasopisma.pan.pl PAN POLSKA AKADEMIA NAUK www.journals.pan.pl

It is assumed that the noise signal satisfies the white noise of normal distribution, i.e.,

$$z_k = \boldsymbol{H} x_k + v_k \,, \tag{28}$$

$$v_k \sim N(Q, R), \tag{29}$$

where the matrix $\boldsymbol{Q}$ is the process noise covariance and the matrix $\boldsymbol{R}$ is the observed noise covariance. $\hat{i}_k^-$ is defined as a priori estimate, that is, the parameter estimate obtained according to the last online calculation result; $\hat{i}_k$ is defined as a posteriori estimate, that is, the parameter estimate obtained according to the current calculation results.

After setting the initial values of filtering and covariance of Kalman filter, the calculation process can be divided into the following steps:

1. The a priori estimate $\hat{i}_k^-$ of the time k is calculated from $\hat{i}_{k-1}$.

$$\hat{i}_k^- = \boldsymbol{A} \hat{i}_{k-1} \,. \tag{30}$$

   At the same time, the covariance matrix $\hat{P}_k^-$ of $\hat{i}_k^-$ is obtained.

$$\hat{P}_k^- = \boldsymbol{A} \hat{P}_{k-1} \boldsymbol{A}^T + \boldsymbol{Q}. \tag{31}$$

2. Calculate the optimal Kalman gain $\boldsymbol{K}_k$.

$$\boldsymbol{K}_k = \hat{P}_k^- \boldsymbol{H}^T \left(\boldsymbol{H} \hat{P}_k^- \boldsymbol{H}^T + \boldsymbol{R} \right)^{-1} . \tag{32}$$

3. The observation vector estimation of the time k is calculated according to a priori estimation $\hat{i}_k^-$.

$$\hat{z}_k^- = \boldsymbol{H} \hat{i}_k^- \,. \tag{33}$$

4. The difference between the parameter estimates z_k and $\hat{z}_k^-$ observed by the IMC observer is calculated, and the a priori estimate $\hat{i}_k^-$ is compensated for to obtain the a posteriori estimate $\hat{i}_k$, that is, the optimal parameter estimate.

$$\hat{i}_k = \hat{i}_k^- + \boldsymbol{K}_k \left(z_k - \boldsymbol{H} \hat{i}_k^- \right) . \tag{34}$$

5. Calculate the a posteriori covariance matrix $\hat{P}_k$.

$$\hat{P}_k = (I - \boldsymbol{K}_k \boldsymbol{H}) \hat{P}_k^- \,. \tag{35}$$

4. Simulation results

In actual working conditions, rise in stator temperature boosts the stator resistance, rise in stator current lowers the stator inductance, while prolonged motor operation may weaken the permanent magnet flux linkage. To verify the effect of the proposed countermeasure in dealing with a motor model mismatch, this paper carried out an experimental verification under two operating conditions, each involving three different circumstances. The controlled object is a surface-mounted PMSM, whose rated parameters are shown in Table 1. The parameters of IMC observers for d-axis and q-axis currents are as follows: $k_1 = -32000$, $k_2 = 50$. The Kalman

Table 1. Parameters of PMSM

Parameter	Rating
Stator resistance/Ω	0.4578
Rotor inertia/kg·m^2	$1.469 \cdot 10^{-3}$
Stator inductance/H	$3.34 \cdot 10^{-3}$
DC bus voltage/V	300
Flux linkage of permanent magnet/Wb	0.171
Rated speed/rpm	2300
Pole pair	4
Rated torque/N·m	14.2

filter system takes $Q = 0.0003$ and $R = 5$. The a-phase current, d-axis current, q-axis current, rotor speed and electromagnetic torque of the motor's stator are denoted by i_a, i_d, i_q, ω_r and T_e, respectively.

Condition 1: Motor running under steady-state operating conditions at a 1500 r/min rotational speed against a 7 N·m given load torque. The sampling took place every $T_s = 100$ µs.

The traditional three-vector MPCC's controlled motor model adopts rated parameters. Experimental waveforms of i_a, i_d, i_q, ω_r and FFT spectrum are as shown in Figs. 6(a)–6(e).

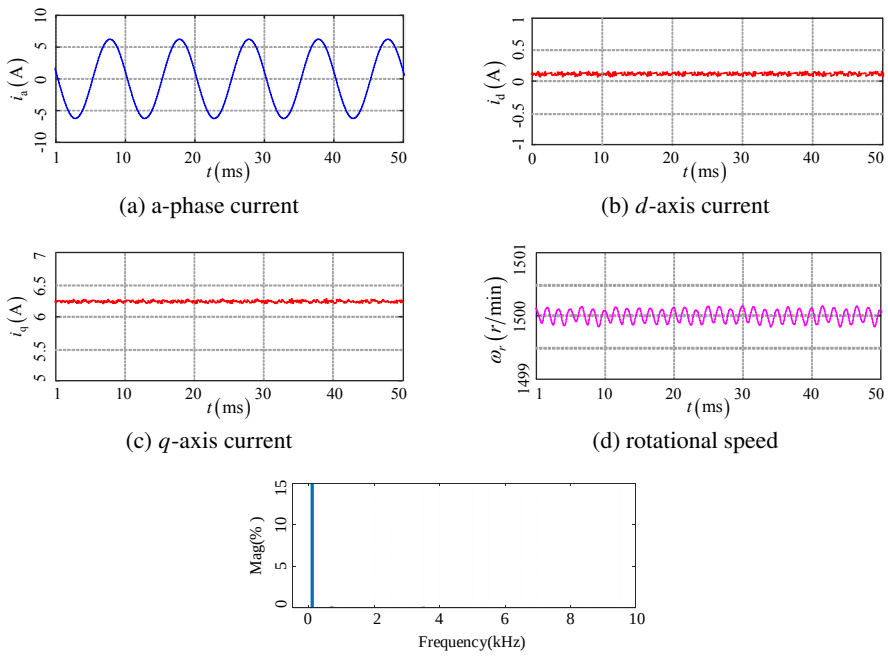

(a) a-phase current (b) d-axis current

(c) q-axis current (d) rotational speed

(e) FFT spectrum of a-phase current

Fig. 6. Experimental waveform of three vector model predictive current control under rated motor parameters

To simulate the actual circumstances of the model mismatch, the model rotor flux linkage was set to 1.1 times the rated value, the model stator inductance to 2 times the rated value, and the model stator resistance to 0.5 times the rated value. Under conditions of the model mismatch, experimental waveforms of i_a, i_d, i_q, ω_r and FFT spectrum are as shown in Figs. 7(a)–7(e), respectively.

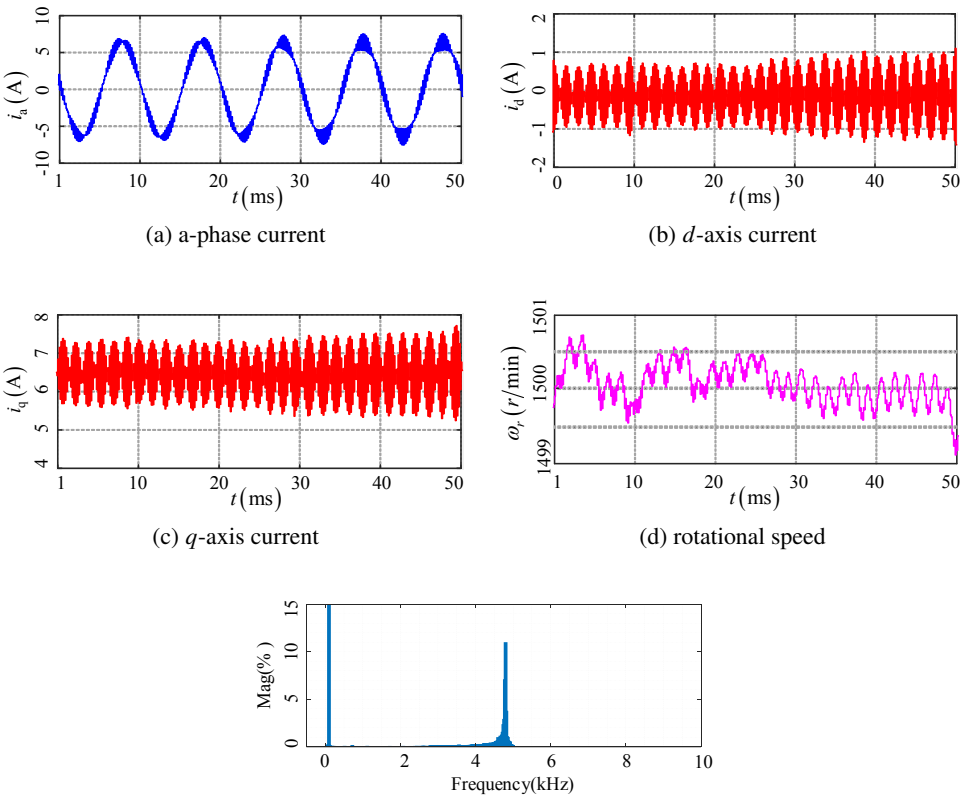

(a) a-phase current (b) d-axis current

(c) q-axis current (d) rotational speed

(e) FFT spectrum of a-phase current

Fig. 7. Experimental waveform of three vector model predictive current control under the condition of motor parameter mismatch

Comparing Fig. 6 and Fig. 7, it could be learned that when actual parameters of the motor deviated further from the model parameters, d-axis and q-axis current fluctuations became more intense, a-phase current distortion became more significant, and rotational speed fluctuation slightly varied. In Fig. 6(e), the THD value of phase current is 0.43%, whereas in Fig. 7(e), the value becomes 14.80%, with more harmonic components appearing near 5 kHz.

Figure 8 shows the results of the motor experiment conducted using the strategy proposed herein under the same mismatch conditions as Fig. 7. It shows that the method could effectively eliminate the impact of mismatched parameters on control performance, and mitigate the para-

metric sensitivity of the MPCC method. The experimental waveforms of i_a, i_d, i_q and ω_r under the proposed strategy are as shown in Figs. 8(a)–8(f), respectively.

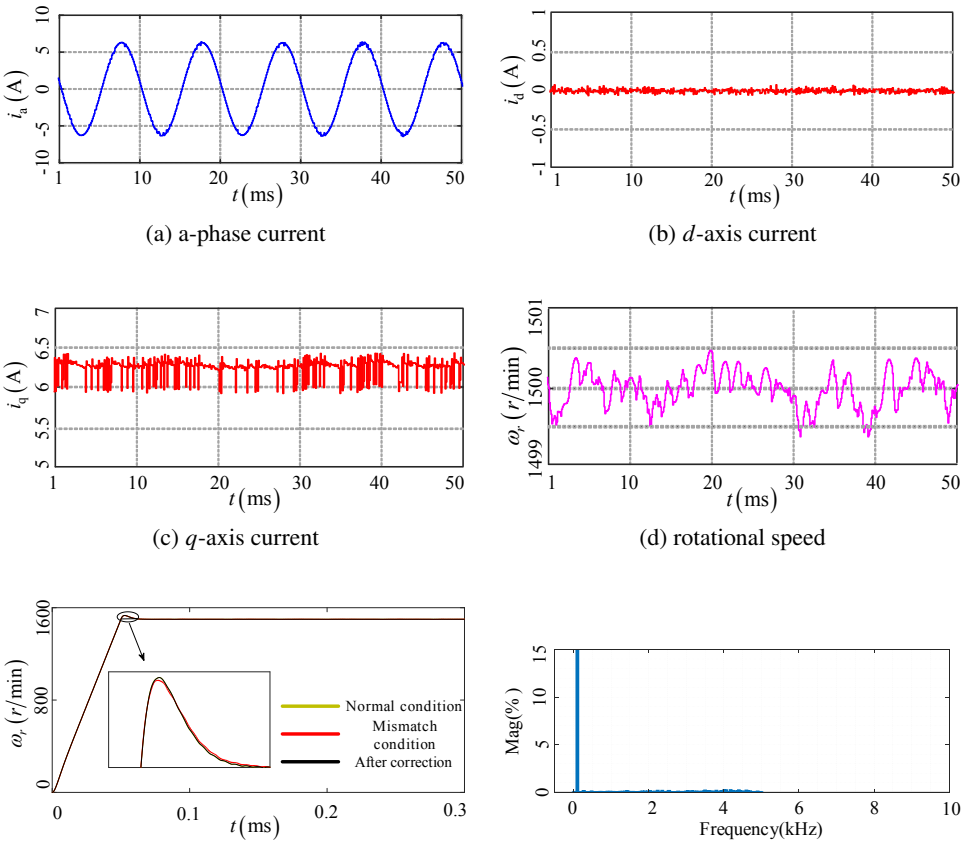

(a) a-phase current (b) d-axis current

(c) q-axis current (d) rotational speed

(e) Speed step response (f) FFT spectrum of a-phase current

Fig. 8. Experimental waveform of three vector model predictive current control based on self-correcting under the condition of motor parameter mismatch

It can be seen from Fig. 8 that, at a steady state, the observation method was able to effectively perform its self-corrective functions in the predictive current control against the PMSM model mismatch. Compared with the mismatch conditions, the corrected d-axis and q-axis currents showed significantly smaller fluctuation, and the distortions of the a-phase current were also ameliorated to some extent. Figure 8(e) shows the speed waveform during motor starting under three working conditions. The speed step response is almost the same as a whole. Compared with the mismatch, the speed curve is smoother under normal and corrected conditions. To vividly depict the harmonic components of the a-phase current, Fig. 8(f) presents the FFT spectrum analysis performed using the method herein. As can be seen from Fig. 8(f), the THD value of the phase current sits at 2.07%, with harmonic components mainly distributed at 0~5 kHz.

www.czasopisma.pan.pl PAN POLSKA AKADEMIA NAUK www.journals.pan.pl

Subsequently, the formulas of current fluctuation coefficients along the d-axis and q-axis were defined as (36) and (37), respectively.

$$\Delta i_d = \sqrt{\frac{1}{N}\sum_{n=1}^{N}(i_d(n) - i_{d_\text{ave}})}, \tag{36}$$

$$\Delta i_q = \sqrt{\frac{1}{N}\sum_{n=1}^{N}(i_q(n) - i_{q_\text{ave}})}, \tag{37}$$

where: i_{d_ave} and i_{q_ave} represent the average of the sampled current of the d-axis and q-axis, respectively; $i_d(n)$ and $i_q(n)$ are the sampled values of the d-axis and q-axis currents; N is the total number of the sample points.

Table 2 lists out the d-axis and q-axis current fluctuation coefficients from Figs. 6–8 as well as the a-phase total harmonic distortion (THD).

Table 2. Current ripple and THD under three conditions of Condition 1

Condition 1	Δi_d	Δi_q	**THD**
Normal condition	0.1327	0.1201	0.43%
Mismatch condition	0.7660	0.7789	14.80%
Internal model control observer	0.4632	0.4050	2.07%

It can be seen from Table 2, that the observation method has effectively reduced the current fluctuation coefficients and THD values under the mismatch condition.

Condition 2: The motor was initiated without any load and ran until the rotational speed reached 500 r/min; at this point, the load torque was stepped from 0 N · m to 7 N · m. The sampling was taken every $T_s = 50$ µs.

Adopting the rated parameters with the traditional three-vector MPCC controlled motor model, the resulting experimental waveforms of i_a, i_d, i_q, ω_r and the FFT spectrum are shown in Figs. 9(a)–9(e), respectively.

The rotor flux linkage of the model was set to 1.1 times the rated value, the model stator inductance to 2 times the rated value, and the model stator resistance to 0.5 times the rated value. Incorporating the model mismatch, the resulting experimental waveforms of i_a, i_d, i_q, ω_r and the FFT spectrum can be seen in Figs. 10(a)–10(e), respectively.

Comparing Fig. 9 and Fig. 10, while also making references to Figs. 6–7, it can be learned that at low rotational speeds, the actual motor parameters deviated from the model parameters, in which case the three-phase current waveform shows significantly greater harmonic distortion, in addition to a significant increase in the d-axis and q-axis current fluctuations. The THD value of the phase current also jumped from 0.41% to 16% in Fig. 9(e) and Fig. 10(e), showing the presence of more harmonic components within a vicinity of 10 kHz.

Under the same mismatch conditions as Fig. 10, the results of the motor experiment conducted using the proposed strategy are presented in Fig. 11. The corresponding experimental waveforms of i_a, i_d, i_q and ω_r are shown in Figs. 11(a)–11(f), respectively.

www.czasopisma.pan.pl PAN POLSKA AKADEMIA NAUK www.journals.pan.pl

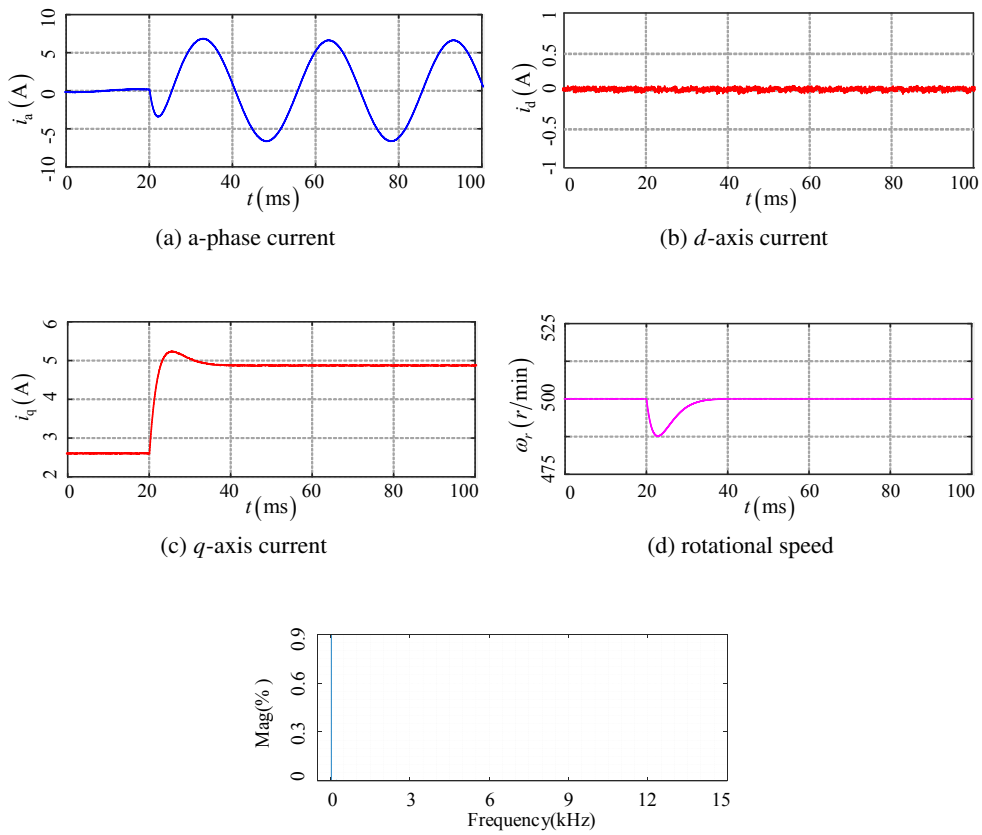

(a) a-phase current (b) d-axis current

(c) q-axis current (d) rotational speed

(e) FFT spectrum of a-phase current

Fig. 9. Waveform of three vector model predictive current control under rated motor parameters

It can be observed from the figures that the proposed method still demonstrated its self-correcting functions in the predictive current control against the model mismatch during the speed regulating stage. Compared with the mismatch conditions, the corrected d-axis and q-axis currents showed significantly smaller fluctuations, with the distortions of the a-phase current also getting considerably lessened. Figure 11(e) shows the speed waveform during motor starting under three working conditions. As can be seen from Fig. 11(e), the response curve fluctuates slightly under mismatch, and the corrected speed step response curve is closer to the curve under normal working conditions. To vividly show the harmonic components of the a-phase current, the FFT spectrum analysis conducted using the proposed method is laid out in Fig. 11(f), showing that the THD value of the phase current sits at 0.52%.

Table 3 enumerates the d-axis and q-axis current fluctuation coefficients from Figs. 9–11 as well as the a-phase THD.

According to Table 3, both the current fluctuation coefficients and THD values under normal conditions and corrected conditions are small relative to the mismatch conditions. This implies

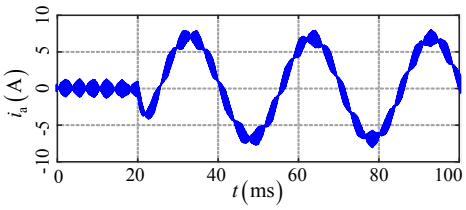

(a) a-phase current

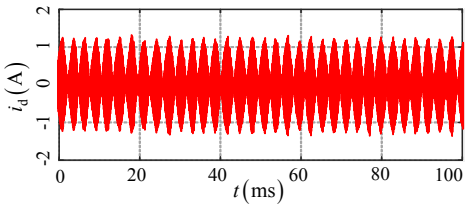

(b) d-axis current

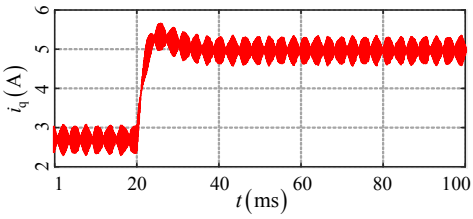

(c) q-axis current

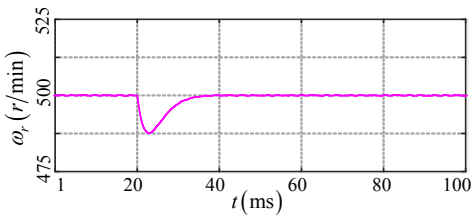

(d) rotational speed

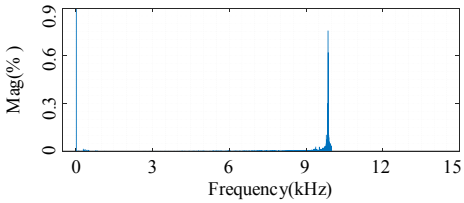

(e) FFT spectrum of a-phase current

Fig. 10. Experimental waveform of three vector model predictive current control under the condition of motor parameter mismatch

Table 3. Current ripple and THD under three conditions of Condition 2

Condition 2	Δi_d	Δi_q	**THD**
Normal condition	0.1333	0.1133	0.41%
Mismatch condition	0.8552	0.8176	16.00%
Internal model control observer	0.1327	0.1449	0.52%

that the observation method proposed herein has significantly reduced the current fluctuation coefficients and THD values under the mismatch condition.

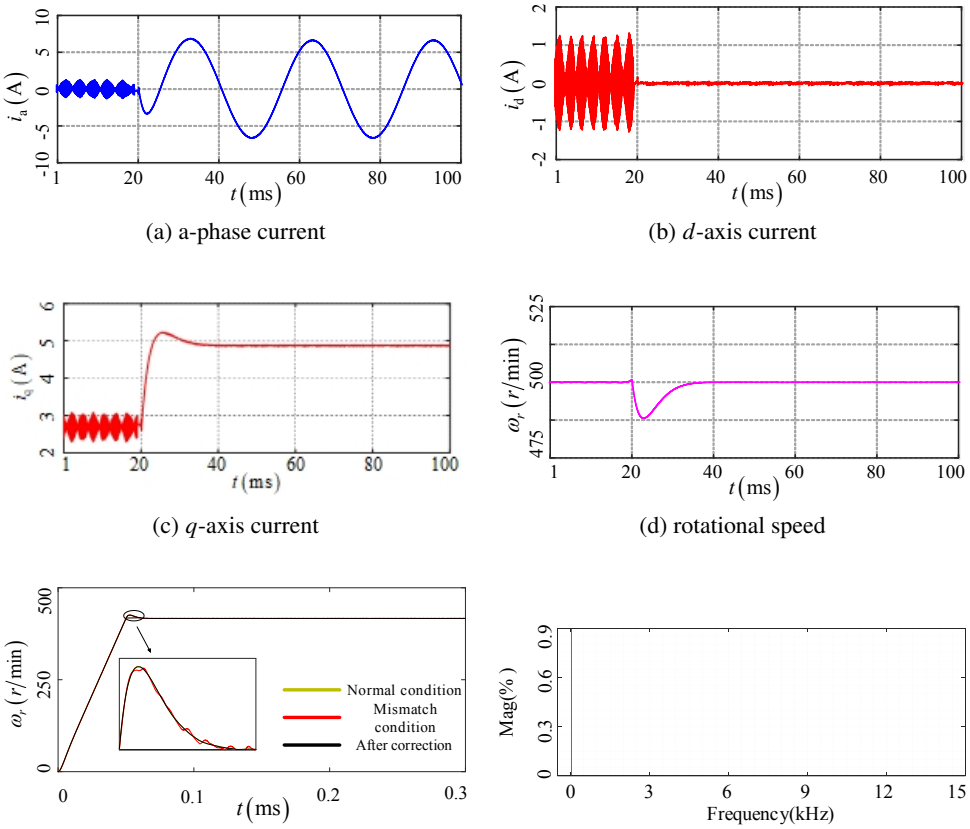

(a) a-phase current (b) d-axis current

(c) q-axis current (d) rotational speed

(e) Speed step response (f) FFT spectrum of a-phase current

Fig. 11. Experimental waveform of three vector model predictive current control based on self-correcting under the condition of motor parameter mismatch

5. Conclusions

This paper introduces an IMC-observer-based method for motor model predictive current control, whose main contributions and advantages can be summarized into the following four aspects:

1. With regards to feasibility, IMC is not only convenient to design and easy to realize, but also boasts a smaller online computational load.
2. In terms of robustness, the IMC-observer-based PMSM predictive current control strategy features a self-corrective function, allowing it to improve the quality of system current waveforms and system robustness under the model mismatch.
3. As for practicality, the IMC-observer-based PMSM predictive current control strategy is applicable under different conditions. At various conditions, be it high and low speeds, or in a steady state and speed regulating stage, the proposed strategy shows satisfactory control performance.

www.czasopisma.pan.pl PAN POLSKA AKADEMIA NAUK www.journals.pan.pl

4. As far as control performance goes, the proposed strategy also shows better control performance, in addition to improving the current fluctuation coefficient and THD value under the mismatch condition.

Regardless of the above superiorities, the proposed IMC observer-based predictive control countermeasure against the PMSM model mismatch also suffers from disturbance in estimation accuracy, whose source of estimation errors has yet to be explored in greater depth in this paper. With that said, analyzing the mechanism of how the estimation error is generated, and optimizing the estimation of disturbance using intelligent algorithms shall become the topic in future works.

Acknowledgements

This research work is supported by National Natural Science Foundation of China (No. 61663021, 61763025, 61861025).

References

[1] Lyskawinski W., *Comparative analysis of energy performance of squirrel cage induction motor, line-start synchronous reluctance and permanent magnet motors employing the same stator design*, Archives of Electrical Engineering, vol. 69, no. 4, pp. 967–981 (2020), DOI: 10.24425/aee.2020.134642.

[2] Pałka R., Piotuch R., *Experimental verification of Dead-Beat predictive current controller for small power, low speed PMSM*, Archives of Electrical Engineering, vol. 67, no. 2, pp. 333–343 (2018), DOI: 10.24425/119644.

[3] Białoń T., Lewicki A., Pasko M., Niestrój R., *Non-proportional full-order Luenberger observers of induction motors*, Archives of Electrical Engineering, vol. 67, no. 4, pp. 925–937 (2018), DOI: 10.24425/aee.2018.124750.

[4] Li Y.H., Qin H., Su J.S., Qin Y.G., Zhao C.H., Zhou Y.F., *Model predictive torque control of permanent magnet synchronous motor based on adaptive dynamic weight coefficient using fuzzy control*, Electric Machines and Control, vol. 25, no. 2, pp. 102–112 (2021), DOI: 10.15938/j.emc.2021.02.012.

[5] Yu F., Zhu C.G., Wu X.X., Zhang L., *Two-vector-based model predictive flux control of three-level based permanent magnet synchronous motor with sector subregion*, Transactions of China Electrotechnical Society, vol. 35, no. 10, pp. 2130–2140 (2020), DOI: 10.19595/j.cnki.1000-6753.tces.190520.

[6] Xu Y.P., Wang J.B., Zhang B.C., Zhou Q., *Three-vector-based model predictive current control for permanent magnet synchronous motor*, Transactions of China Electrotechnical Society, vol. 33, no. 5, pp. 980–988 (2018), DOI: 10.19595/j.cnki.1000-6753.tces.170044.

[7] Zhang H., Zhang Y.C., Liu J.L., Gao S.Y., *Model-free predictive current control of permanent magnet synchronous motor based on single current sampling*, Transactions of China Electrotechnical Society, vol. 32, no. 2, pp. 180–187 (2017), DOI: 10.19595/j.cnki.1000-6753.tces.2017.02.021.

[8] Elumalai V.K., Subramanian R.G., Reddipogu J.S.D., *Enhanced IMC synthesis for tracking control of magnetic levitation system*, Archives of Electrical Engineering, vol. 67, no. 2, pp. 293–306 (2018), DOI: 10.24425/119641.

[9] Ogbuka C., Nwosu C., Agu M., *Dynamic and steady state performance comparison of line-start permanent magnet synchronous motors with interior and surface rotor magnets*, Archives of Electrical Engineering, vol. 65, no. 1, pp. 105–116 (2016), DOI: 10.1515/aee-2016-0008.

[10] Rolek J., Utrata G., Kaplon A., *Robust speed estimation of an induction motor under the conditions of rotor time constant variability due to the rotor deep-bar effect*, Archives of Electrical Engineering, vol. 69, no. 2, pp. 319–333 (2020), DOI: 10.24425/aee.2020.133028.

www.czasopisma.pan.pl PAN POLSKA AKADEMIA NAUK www.journals.pan.pl

[11] Verrelli C.M., Savoia A., Mengoni M., Marino R., Tomei P., Zarri L., *On-line identification of winding resistances and load torque in induction machines*, IEEE Transactions on Control Systems Technology, vol. 22, no. 4, pp. 1629–1637 (2014), DOI: 10.1109/TCST.2013.2285604.

[12] Jin B.L., Shen Y.X., Wu D.H., *Permanent magnet synchronous motor parameter identification with multi-innovation least squares*, Proceedings of the 2016 IEEE 11th Conference on Industrial Electronics and Applications, Wuxi, China, pp. 752–757 (2016).

[13] Chen H., Hao R.X., Liu Y.Y., Wang H., Wang T.X., Li D.L., *Parameter identification of time-varying exponential load model based on improved RLS algorithm*, High Voltage Engineering, vol. 46, no. 7, pp. 2380–2388 (2020), DOI: 10.13336/j.1003-6520.hve.20200310013.

[14] Xie S.W., Xie Y.F., Huang T.W., Gui W.H., Yang C.H., *Generalized predictive control for industrial processes based on neuron adaptive splitting and merging RBF neural network*, IEEE Transactions on Industrial Electronics, vol. 66, no. 2, pp. 1192–1202 (2019), DOI: 10.1109/TIE.2018.2835402.

[15] Fan Z.F., Ma X.P., Shao X.G., *Method to determine initial value of local optimization forneural network predictive control*, Control Theory and Applications, vol. 31, no. 6, pp. 741–747 (2014), DOI: 10.7641/CTA.2014.31262.

[16] Yuan L., Wen T.S., Sen C., Jun F.J., *Research and application of predictive control algorithm based on fuzzy model*, 2015 International Conference on Advanced Mechatronic Systems, Beijing, China, pp. 244–248 (2015).

[17] Seddjar A., Kerrouche K.D.E., Wang L., *Simulation of the proposed combined Fuzzy Logic Control for Maximum Power Point Tracking and Battery Charge Regulation used in Cube Sat*, Archives of Electrical Engineering, vol. 69, no. 3, pp. 521–543 (2020), DOI: 10.24425/aee.2020.133916.

[18] Qin Y.Z., Yan Y., Chen W., Geng Q., *Three-vector model predictive current control strategy for permanent magnet synchronous motor drives with parameter error compensation*, Transactions of China Electrotechnical Society, vol. 35, no. 2, pp. 255–265 (2020), DOI: 10.19595/j.cnki.1000-6753.tces.181693.

[19] Siami M., Khaburi D.A., Rodriguez J., *Torque ripple reduction of predictive torque control for PMSM drives with parameter mismatch*, IEEE Transactions on Power Electronics, vol. 32, no. 9, pp. 7160–7168 (2017), DOI: 10.1109/TPEL.2016.2630274.

[20] Huang Y.W., Xiong S.H., *An internal model control-based observer for current loops in permanent magnet synchronous motor*, Proceedings of the CSEE, vol. 36, no. 11, pp. 3070–3075 (2016), DOI: 10.13334/j.0258-8013.pcsee.2016.11.024.

[21] Jia Q., Xia C., *Exponential stability of impulsive delayed nonlinear hybrid differential systems*, Archives of Electrical Engineering, vol. 68, no. 3, pp. 553–564 (2019), DOI: 10.24425/aee.2019.129341.